DOI: 10.37190/ ABB-02300-2023-01

A novel electrode to achieve balance between anastomotic strength and tissue thermal damage for radiofrequency-induced intestinal anastomosis

Xupo Xing, Chengli Song*

Shanghai Institute for Minimally Invasive Therapy, School of Health Science and Engineering, University of Shanghai for Science and Technology, Shanghai, China.

Corresponding author: Chengli Song, Shanghai Institute for Minimally Invasive Therapy, School of Health Science and Engineering, University of Shanghai for Science and Technology, China, 200093, e-mail address: csong@usst.edu.cn

Submitted: 21st August 2023

Accepted: 13th October 2023

Abstract

Purpose: This paper aimed to develop a novel electrode to achieve balance between anastomotic strength and tissue thermal damage for radiofrequency-induced intestinal anastomosis.

Methods: The mechanical properties of the novel electrode were analyzed by finite element method, and then the temperature and thermal damage distribution of intestinal tissue during welding process were analyzed by electric-thermal-mechanical multi-field coupled finite element analysis. In ex-vivo experiments, the biomechanical strength of anastomotic area was assessed by indexes of tensile force and burst pressure. A thermocouple probe and an infrared thermal imager were used to monitor the temperature and thermal damage of the intestinal tissue in experiments. Furthermore, histopathological examination and transmission electron microscopy observation were used to observe the morphology and microstructural of anastomotic area.

Results: A slightly higher mean biomechanical strength is acquired with the tensile force and burst pressure results increasing from 9.7 ± 1.47 N, 84.0 ± 5.99 mmHg to 11.8 ± 2.01 N, 89.6 ± 6.79 mmHg respectively as well as the percentage of necrotic tissue caused by thermal damage decreasing from 89% to 33% for the novel electrode group, with compression force of 20 N, radiofrequency(RF) energy of 120 W and welding duration of 8 s applied to the target regions to achieve anastomosis. Moreover, tightly connected intestinal tissue with collagenic crosslink in the fusion area could be observed by histopathological examination and transmission electron microscopy.

Conclusion: Our study shows that the proposed novel electrode could achieve balance between anastomotic strength and tissue thermal damage for radiofrequency-induced intestinal anastomosis.

Keywords: radiofrequency energy, novel electrode, tissue fusion, anastomotic strength, tissue thermal damage

1 Introduction

Colorectal cancer is a common malignant tumor in humans, and its morbidity and mortality are at the forefront of malignant tumors [21]. At present, an effective clinical treatment method is to resect the diseased intestinal tract through surgery, and then anastomose the remaining stump tissues to reconstruct the continuous structure of the intestinal tract and finally restore its physiological function [6], [12]. Compared with traditional tissue anastomosis methods such as suturing and stapling which are confronted with possible complications of bleeding and leakage, radiofrequency (RF) intestinal welding technology has obvious advantages, because it can achieve a rapid bond between the native tissues, and realize the seamless connection of tissues, and reduce the infection of tissues [1], [10], [23].

However, the application of RF tissue welding technology in intestinal anastomosis suffers some problems such as serious tissue thermal damage and insufficient anastomotic strength. For most RF-induced intestinal anastomosis cases that have high biomechanical strength of the fused areas, they usually face severe tissue thermal damage [5], [30]. Thus, it is vital to obtain balance between anastomotic strength and tissue thermal damage for radiofrequency-induced intestinal anastomosis.

With further development of the RF tissue welding technology, different electrode structures and combinations of various welding parameters such as RF energy output power, welding duration, and compression pressure have been investigated to minimize tissue thermal damage during the welding process [19]. Zhao et al. designed a traditional copper electrode with a smooth surface called S electrode and a novel copper electrode named CC electrode and compared the performance of the two types of electrodes in RF-induced intestinal anastomosis using indices of burst pressure and thermal diffusion profiles. And the results show that the CC electrode group behaved with higher burst pressure and smaller thermal diffusion profile compared with the S electrode group indicating that appropriate electrode structure can achieve better welding [30].

Hu et al. investigated the influence of different welding parameter combinations on the performance of RF tissue fusion. And the results show that under the optimal combination of welding parameters with the energy output power, compression pressure and welding time were 160 W, 995 kPa, and 13 s, respectively, and an intact microstructure with little free collagen in the fused area could be observed [11]. Tu et al. devised a self-cooling electrode to reduce tissue thermal lesions by rinsing the tissue with 0.9% saline during the welding process. Histological observation results indicate that the designed self-cooling electrode can reduce tissue thermal damage [24]. The above studies have confirmed that the application of RF energy for intestinal

tissue welding is feasible and various rational methods can be used to achieve balance between anastomotic strength and tissue thermal damage.

At present, the materials of RF tissue welding electrodes are basically copper alloy, which are excellent metal conductors with electrical conductivity of 5.998e7 ($S \cdot m^{-1}$), and thermal conductivity of 400 ($W \cdot m^{-1} \cdot K^{-1}$). However, copper alloy is non-biodegradable and it is not suitable for clinical use due to cavity physiological characteristics of intestinal and welding methods shown in Figure 1. The development of RF tissue welding technology was limited by the non-degradability of previous RF tissue welding electrodes. Magnesium alloy is known as a revolutionary biomedical material with the advantages of good mechanical properties, biocompatibility, and biodegradability, which has potential application value as tissue welding electrodes [8], [14], [15]. Furthermore, nanocoating on magnesium alloy could facilitate tissue regeneration [13], [26].

The finite element method is widely used in the medical field [16], [25]. Thus, this paper proposed a novel degradable magnesium alloy electrode with hollow structure compared to the conventional electrode (Ring electrode) to achieve balance between anastomotic strength and tissue thermal damage for RF-induced intestinal anastomosis. The performance of the proposed novel electrode was assessed by experiments and finite element analysis.

To assess the performance of the novel electrode in RF-induced intestinal anastomosis, this paper explores the tissue temperature distribution and tissue thermal damage during the welding process through mechanical-electro-thermal multi-field coupled finite element analysis. Moreover, the biomechanical strength, temperature changes, and microstructure of the fused intestinal tissues were further investigated and validated through ex-vivo experiments.

2 Materials and methods

2.1 Mechanical structure design

The mechanical structure and working flow chart of the novel electrode are displayed in Figure 1. The designed novel electrode is placed in the intestinal lumen as negative electrode and used to execute end-to-end anastomosis between two separate segments of intestinal tissue in the order of “mucosa-serosa”, and then RF energy is applied to complete the welding. After fusion, the novel electrode degraded. The material of the novel electrode consists of Mg-Nd-Zn-Zr (named JDBM) developed by Shanghai Jiao Tong University, which is safe for humans [2].

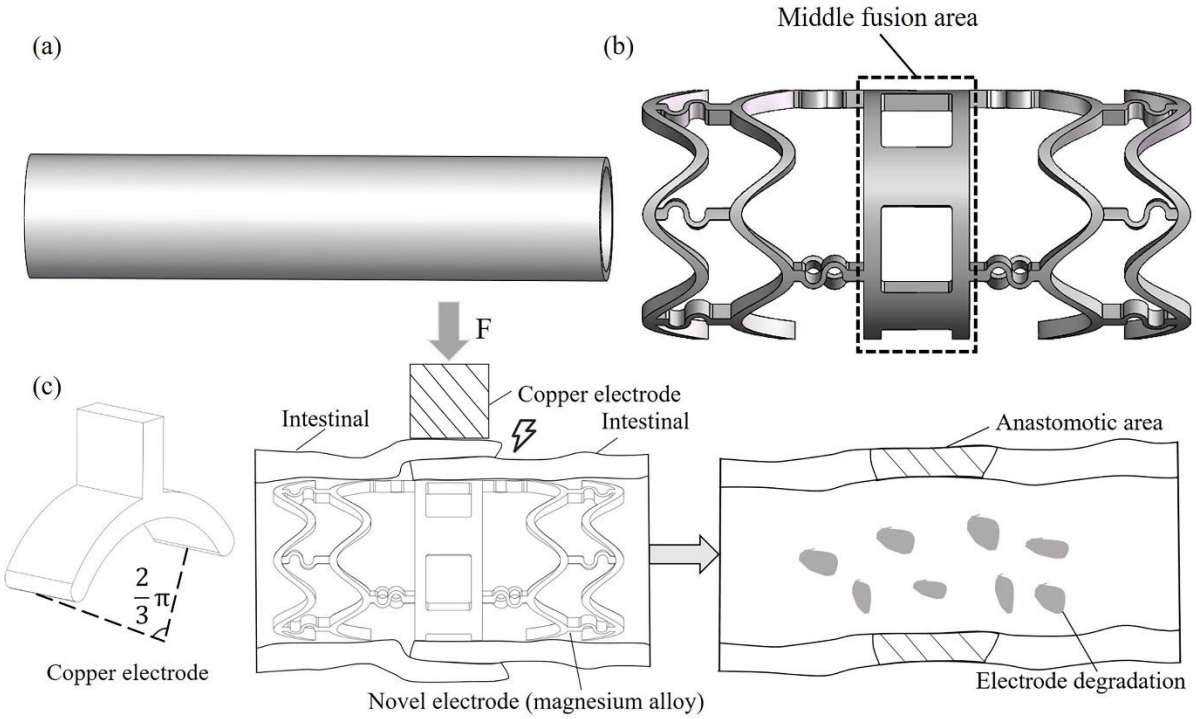

Figure.1 Mechanical structure and working flow chart of the novel electrode (a) Mechanical structure of traditional Ring electrode (b) Mechanical structure of novel electrode (c) Working flow chart of the novel electrode.

2.2 Finite element analysis

2.2.1 Mechanical properties of the novel electrode

Since the electrode will receive certain pressure during the tissue welding process, the mechanical properties of the novel electrode are investigated through finite element analysis. In experiments, the discrete linkage-type welding device developed by our group (China Patent ZL 2018 1 0891397.6) is used for tissue fusion. The discrete linkage-type welding device consists of three identical discrete copper electrodes, each spanning an angle of 120 degrees (Figure 1. c (left)). In experiments, the force was applied to the discrete copper electrodes, then RF energy was applied to complete the fusion (Figure 1. c, Figure 3. a).

To be consistent with the force mode of the novel electrode in the experiments, the outermost surface of the middle fusion area of the novel electrode was divided into two areas by one-third and two-thirds from the circumferential direction using SOLIDWORKS 2016 software. ANSYS 19.2 software is used for the mechanical analysis of the novel electrode. In the boundary condition setting of the finite element model, a total force of 20 N is loaded to one-third of the middle fusion area of the novel electrode, as shown in Figure 2. By turning on

the "weak spring" and "inertial release" operations in the software, the novel electrode was restrained and kept in a state of force balance.

2.2.2 Temperature distribution and tissue thermal damage

The temperature distribution and tissue thermal damage during the welding process were obtained by the mechanical-electro-thermal multi-field coupled finite element analysis.

Construction of fusion model

Since the welding performance is mainly related to the middle fusion area, the novel electrode is simplified and the geometry structure of the two electrodes is identical except the intermediate area for intestinal tissue welding. Mechanical-electro-thermal multi-field coupled finite element model is shown in Figure. 3. And the two layers of intestinal tissue are simplified as one cylinder with an outer diameter of 20 mm and an inner diameter of 14 mm.

Governing equations

After completing the above-mentioned finite element models built in SOLIDWORKS 2016, COMSOL 6.0 software is used to execute mechanical-electro-thermal multi-field coupled finite element analysis.

The viscoelastic properties of intestinal tissue can be expressed by the Maxwell model expressed in Equation 1 [29].

$$\dot{\varepsilon} = \frac{\dot{\sigma}}{E} + \frac{\sigma}{\eta} \tag{1}$$

Where ε is strain, σ represents stress, E denotes elastic modulus, and η is viscosity coefficient, respectively.

The physical phenomena of the thermoelectric coupling problem follow the Pennes biological heat transfer equation [18].

$$\rho c \frac{\partial T}{\partial t} = \nabla \cdot (k \nabla T) + \rho_b c_b \omega (T_b - T) + Q \tag{2}$$

Where ρ represents density, c denotes specific heat, k is thermal conductivity, T indicates temperature, T_b is arterial temperature, ρ_b is blood density, c_b represents blood specific heat, ω denotes blood perfusion rate, and Q is power absorption, respectively.

Tissue thermal damage is calculated by the Arrhenius equation as expressed below [17]:

$$\Omega(\tau) = \int_0^\tau A e^{\frac{-E_a}{RT}} dt \tag{3}$$

Where $\Omega(\tau)$,τ, A, and E_a are the degree of tissue injury, heating time, frequency factor, and

activation energy, respectively.

Boundary conditions and material properties

In the experiments, the RF power with sinusoidal output voltage was provided by the LigaSure TM vessel sealing system (Valleylab, Covidien, USA) for tissue fusion. The measured sinusoidal output voltage by an oscilloscope (Tektronix, TPS2024B) was converted to the corresponding root mean square (RMS) value of the direct current voltage with the value of 102 V and the duty cycle of 60% for enhancing the convergence of the finite element model [28]. And the converted direct current voltage was loaded on the positive electrode and the zero voltage was loaded on the negative electrode. The total simulation time was 8 seconds. At t=0, the intestinal tissue temperature was set to 37 °C, and the environment temperature was set to 25 °C. The heat dissipation coefficient of the air-tissue interface was set to 10 ($W \cdot m^{-1} \cdot K^{-1}$).

The material properties for finite element analysis are listed in Table 1. The material of the positive electrode is copper and the material of the negative electrodes (Ring electrode and novel electrode, separately) is biodegradable magnesium alloy (Mg-Nd-Zn-Zr). The electrical conductivity σ_{normal}, the thermal conductivity k of intestinal tissue, and the electrical conductivity σ_* of compressed intestinal tissue were considered temperature-dependent piecewise functions expressed as Equation 4-6 [3], [4], [22].

$$\sigma_{normal} = \begin{cases} 0.28\times\left(1 + 0.015\times(T - 37)\right) & T \le 100 \\ 0.6384 & T > 100 \end{cases} \quad (4)$$

$$\sigma_* = \begin{cases} 0.07\times\left(1 + 0.015\times(T - 37)\right) & T \le 100 \\ 0.1596 & T > 100 \end{cases} \quad (5)$$

$$k = \begin{cases} 0.54\times\left(1 + 0.015\times(T - 37)\right) & T \le 100 \\ 1.05 & T > 100 \end{cases} \quad (6)$$

2.3 Welding experiment

Fresh porcine small intestine fragments 50-60 mm in length were used as specimens for welding experiments. The RF power was provided by the LigaSure TM vessel sealing system (Valleylab, Covidien, USA) for tissue fusion (Figure. 4).

Two layers of intestinal tissue are placed on the surface of the novel electrode in the order of “mucosa-serosa”. The compression force is always kept at 20 N with approximately

corresponding pressure of 20 kPa in welding experiments since the anastomotic area would rupture under the condition of higher compression pressure. Different combinations of welding parameters (Table 2) are performed in the experiments to assess the ability of the novel electrode in RF-induced intestinal anastomosis. Each experimental group was repeated five times.

The temperature of intestine tissue during the welding process is a key factor to achieve high-quality anastomosis. When the temperature is too low, intestinal tissue cannot be effectively welded, however, if the temperature is too high, it may cause serious tissue thermal damage. So, a thermocouple probe and an infrared thermal imager were used to monitor the temperature during the welding process in the experiments. The position of the thermocouple probe is consistent with the position of the domain point probe in the finite element model. The thermocouple probe is used to monitor the temperature of a specific point and an infrared thermal imager is used to monitor the temperature of the surface of the intestinal tissue welding area. For the infrared thermal imaging monitoring results, the area with temperature higher than 60 ℃ is considered to suffer tissue thermal damage [7].

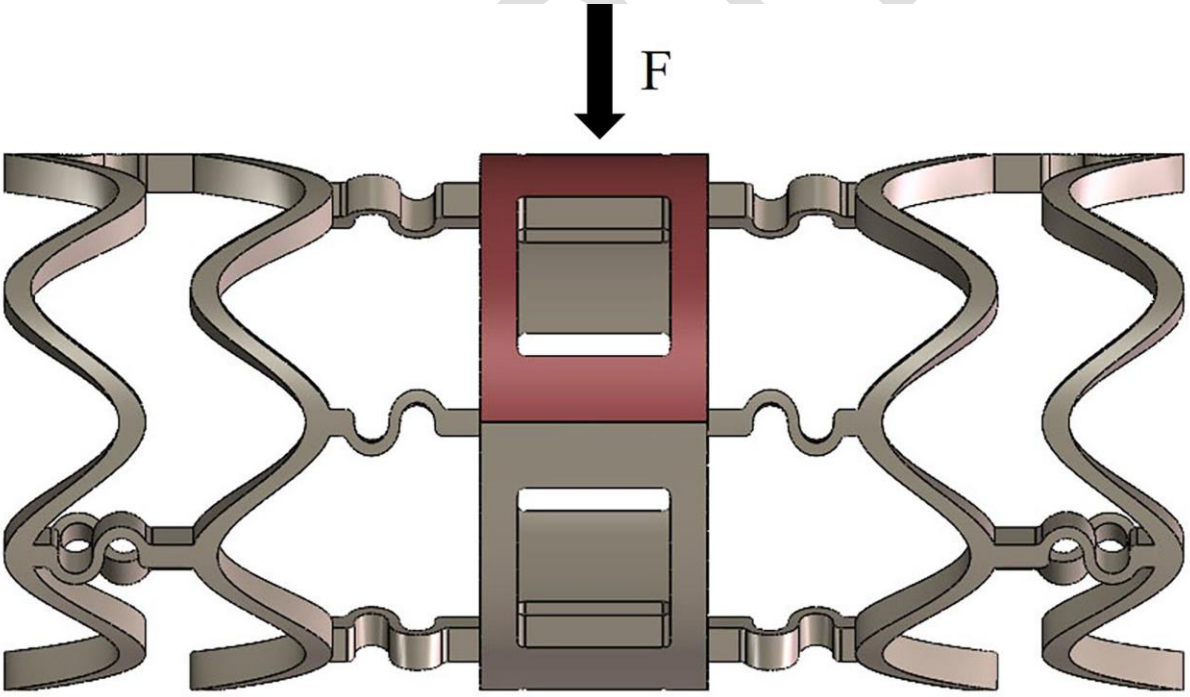

Figure.2 Schematic diagram of force loading method.

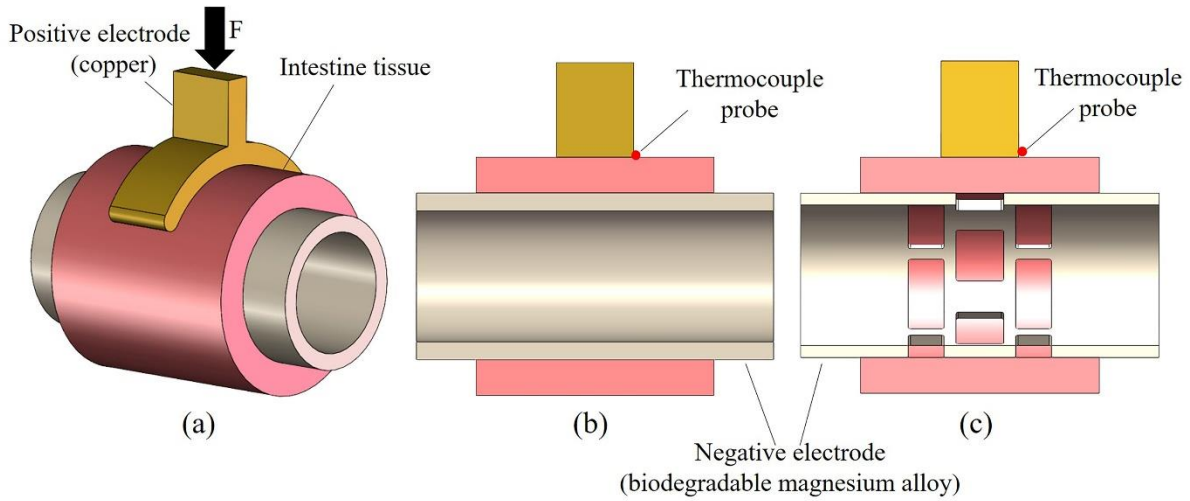

Figure.3 Geometry of the finite element model for temperature distribution and tissue thermal damage. (a) The overall chart of the finite element model. (b) The fusion model of the traditional Ring electrode. (c) The fusion model of the novel electrode.

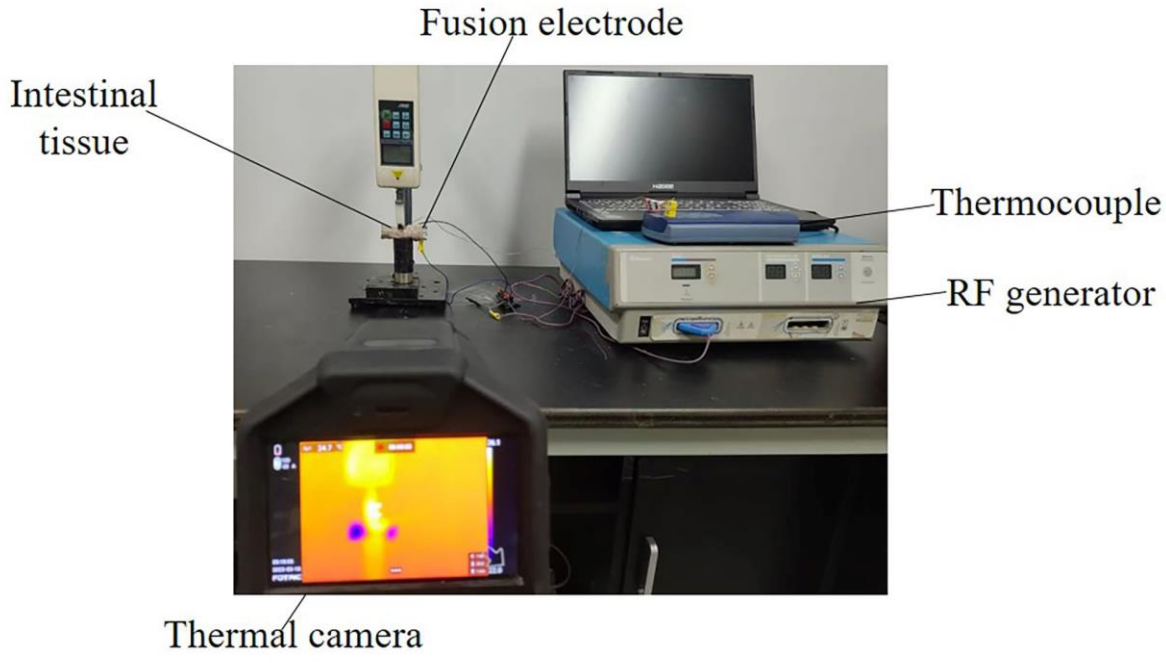

Figure.4 Intestinal tissue fusion platform.

2.4 Mechanical strength test of anastomotic area

Burst pressure test and tensile force test are used as indexes for evaluating anastomotic strength (Figure. 5). In the burst pressure test, 0.9% saline was injected into the fused intestinal tissue at a constant speed of 1ml/min, and the pressure value was recorded as the anastomotic

area began to leak (Figure. 5 a). In the tensile force test, one end of the anastomotic intestinal tissue is fixed, and the other end is connected to a digital force gauge. Then, the anastomotic intestinal tissue was slowly stretched, and the peak force value was recorded as the anastomotic area ruptured. To better assess the performance of the proposed novel electrode, the tensile force of normal intestinal tissue was acquired by a universal testing machine (INSTRON5965, America). Under the same combination of welding parameters, i.e. the same experimental group (Table 2), the results of tensile force and burst pressure tests were compared by the Mann–Whitney U test using SPSS 19 software.

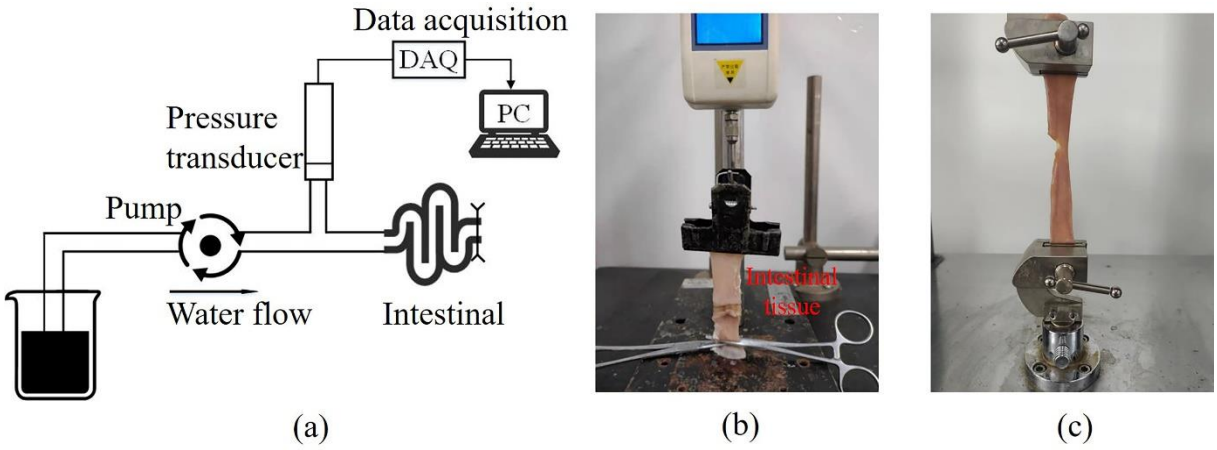

Figure.5 Strength test of anastomotic area (a) Schematic diagram of burst pressure test (b) Tensile force test of the fused intestinal tissue (c) Tensile force test of normal intestinal tissue.

2.5 Histopathological observation and ultrastructural characterization

After being fixed, embedded, and stained with hematoxylin and eosin (H&E) in sequence, the anastomotic area under the condition of optimal welding parameter combination (Table 2, group 1), i.e. the anastomotic area which performed the highest biomechanical strength was observed by a light microscope (DMi8, Leica, Germany). Ultrastructure changes such as collagen morphological transition in the anastomotic area under the condition of optimal welding parameter combination were investigated by transmission electron microscopy (HT7700, HITACHI, Japan).

3 Results

3.1 Mechanical properties of the novel electrode

Finite element analysis results of the novel electrode after loading pressure are shown in Figure. 6. The maximum deformation of the novel electrode is 0.11 mm, and the maximum Von Mises stress is 154.75 MPa.

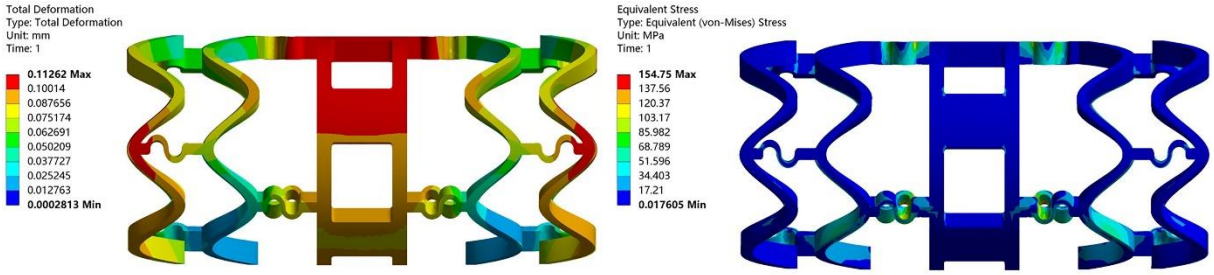

(a) (b)

Figure.6 Finite element analysis results of the novel electrode after loading pressure (a) Deformation contour of the novel electrode (b) Von Mises stress contour of the novel electrode.

Table 1 Physical parameters of the materials [3], [4], [22]

Parameter	Intestinal tissue	Copper	Magnesium alloy
ρ ($kg \cdot m^{-3}$)	1088	8960	1770
μ	0.49	0.35	0.35
E (MPa)	1.84	1.1×10^{5}	4.5×10^{4}
σ ($S \cdot m^{-1}$)	0.28, 0.07 *	5.99×10^{7}	6.41×10^{6}
ε	2430	1	1
C ($J \cdot kg^{-1} \cdot K^{-1}$)	3665	385	1000
k ($W \cdot m^{-1} \cdot K^{-1}$)	0.54	400	105.22

Note: σ and k are measured at the temperature of 37°C and * denotes the corresponding parameters of the compressed intestinal tissue.

Table 2 Experiment parameters of radiofrequency-induced tissue fusion

Group	RF energy output power (W)	Welding duration (s)	Compression force (N)
1	120	8	20
2	120	10	20
4	140	6	20
5	140	8	20
6	160	6	20
7	160	8	20

3.2 Biomechanical properties of anastomotic area

The prototype of the novel electrode is shown in Figure.7.a (down). The biomechanical strength of anastomotic area welded by the novel electrode was slightly higher than that of the Ring electrode. The anastomotic area achieved the highest biomechanical strength with the tensile force of 11.8±2.01 N and burst pressure of 89.6±6.79 mmHg under welding parameter combinations of compression force of 20 N, RF energy of 120 W, and welding duration of 8 s (Figure.7.b). To better assess the performance of the proposed novel electrode, the tensile force of normal intestinal tissue was acquired with the approximate maximum of 23 N (Figure.7.c). The maximum deformation of intestinal tissue in the anastomosis area is 0.05 mm (Figure.7 (d-e)).

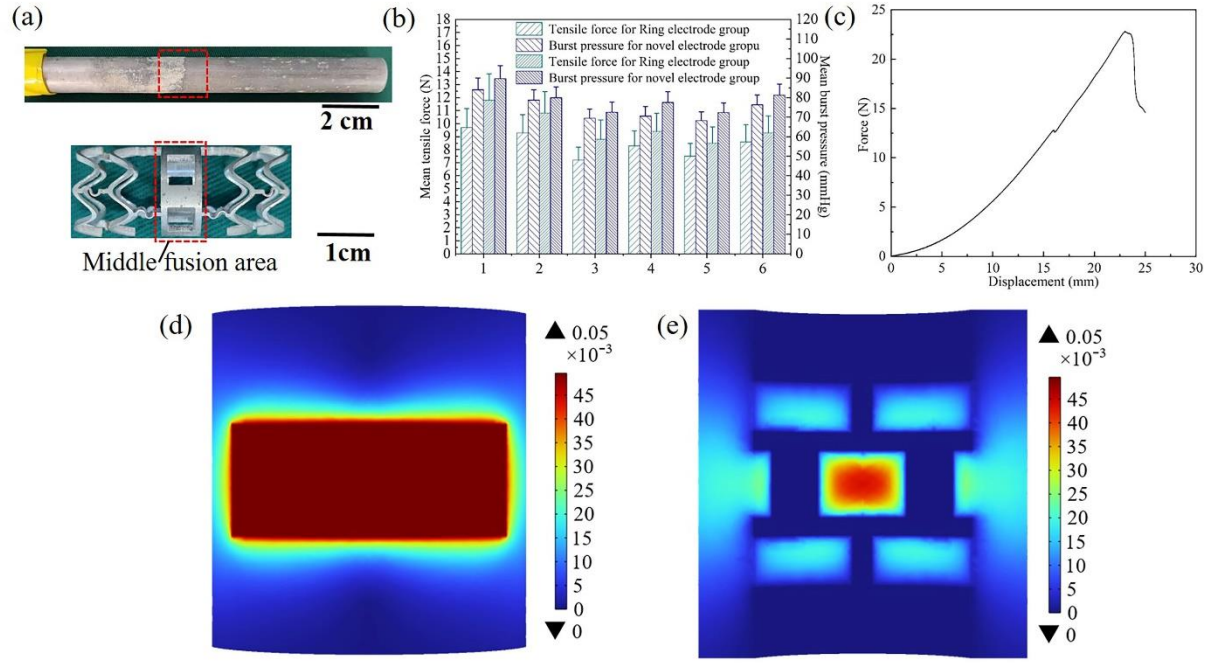

Figure.7 Prototype of the novel electrode and biomechanical strength of intestinal tissue (a) Prototype of the Ring electrode (up), prototype of the novel electrode (down) (b) Mechanical strength test results of the anastomotic area (c) Tensile force test result of normal intestinal tissue. (d) Top view of intestinal tissue deformation in the anastomosis area for the novel electrode fusion model. (e) The sectional view of intestinal tissue deformation in the anastomosis area for the novel electrode fusion model.

3.3 Temperature distribution and tissue thermal damage

In the post-processing of the finite element results, the intestinal tissue is segmented and resected along the XOY plane, XOZ plane, and YOZ plane in turn, and only one-eighth of the original intestinal tissue is retained. The temperature distribution contours of intestinal tissue

during the welding process are displayed in Fig. 8 (a-b). The highest temperature during the welding process is 124 °C for the Ring electrode fusion model and 118 °C for the novel electrode fusion model. The highest temperature occurs at the junction of the compressed area and the uncompressed area of the intestinal tissue. The error between the temperature of the thermocouple probe in the welding experiments and the temperature of the domain point probe in the finite element analysis is lower than 8%, which indicates that the established finite element model is reliable. And the area of intestinal tissue with temperature above 60 °C during the fusion process is defined as an effective welding area for intestinal anastomosis [9].

The thermal damage contours of intestinal tissue during the fusion process acquired by the finite element method are displayed in Figure. 9. At t =8 s, the percentage of necrotic tissue in the welding area is about 89% for the Ring electrode fusion model and 33% for the novel electrode fusion model. In the experiment, the thermal damage range (1.69±0.1 mm) was observed for the Ring electrode group and 1.40±0.1 mm for the novel electrode group.

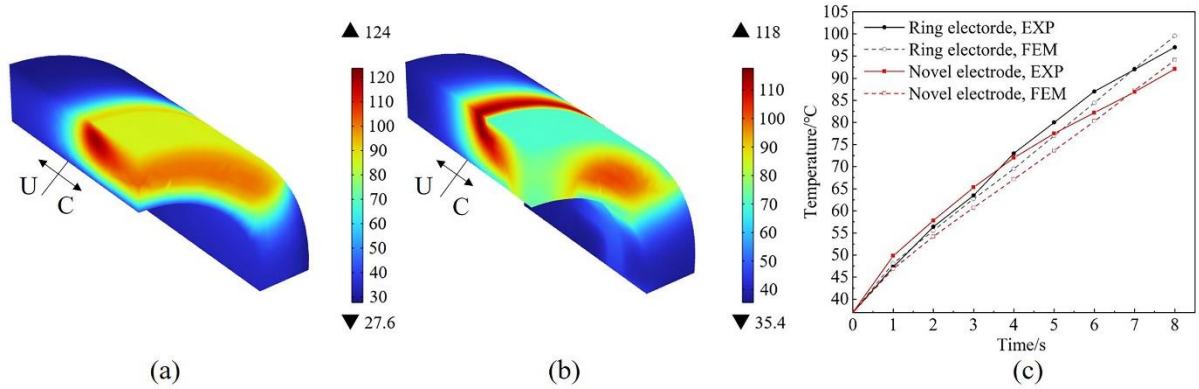

Figure.8 Temperature distribution contours of intestinal tissue fused under the condition of compression force of 20 N, RF energy of 120 W, and welding duration of 8 s. (a) Temperature distribution contours of intestinal tissue fused by Ring electrode (b) Temperature distribution contours of intestinal tissue fused by the novel electrode (c) The curve of the temperature of the domain point probe in finite element model and thermocouple probe in the experiment, respectively. C, intestinal tissue under compression by the two electrodes; U, uncompressed intestinal tissue.

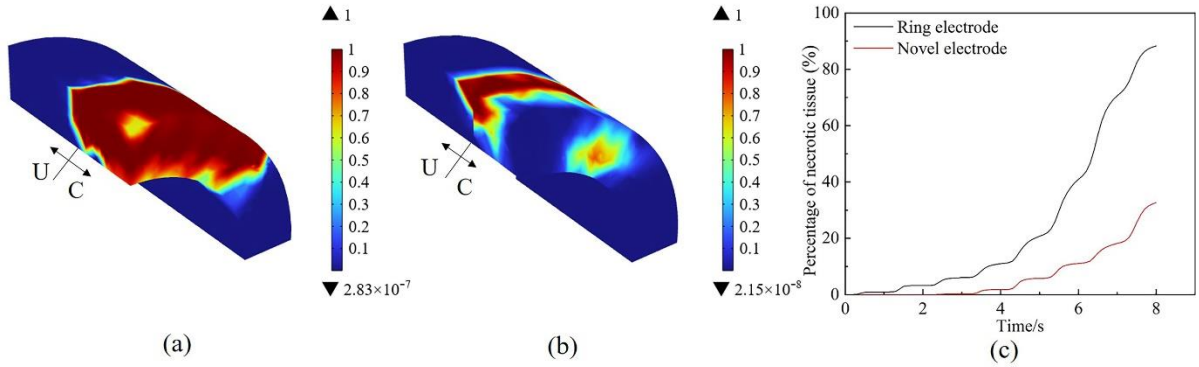

Figure.9 Tissue thermal damage under the condition of compression force of 20 N, RF energy of 120 W, and welding duration of 8 s. (a) Tissue thermal damage distribution contours of intestinal tissue fused by Ring electrode (b) Tissue thermal damage distribution contours of intestinal tissue fused by the novel electrode (c) Percentage of necrotic tissue. C, intestinal tissue under compression by the two electrodes; U, uncompressed intestinal tissue.

3.4 Histopathological examination and ultrastructural analysis of anastomotic area

Histopathological observations of normal intestinal tissue and anastomosis area under optimal welding parameter combination of compression force of 20 N, RF energy of 120 W, and welding duration of 8 s (Table 2, group 1) are displayed in Figure. 10. Compared with normal intestinal tissue with clear layered structure of serosa, muscle layer, sub-mucosa, and mucosa respectively, the fusion area of the two-layer intestinal tissue is more tightly connected with decreased thickness indicating a satisfactory connection between the opposing tissues.

Ultrastructural characterizations of normal intestinal tissue and anastomosis area under optimal welding parameter combinations of compression force of 20 N, RF energy of 120 W, and welding duration of 8 s (Table 2, group 1) observed by transmission electron microscope with 6,000 times magnification are shown in figure.11. Compared with the fine and regular arrangement of collagen fibers in the transverse and longitudinal directions of normal intestinal tissue, the collagen fibers in anastomosis area appear distorted with wider gaps between each collagen fibril which provides an opportunity to facilitate sufficient precipitation and crosslink of proteins and consequently generating strong bonds.

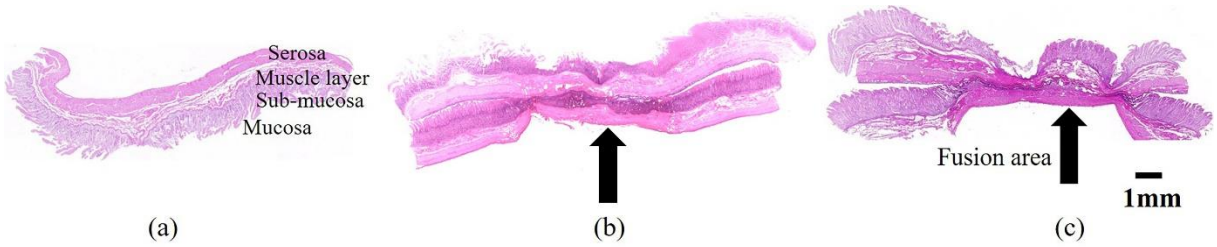

Figure.10 Histopathological examination of anastomosis area. (a) Normal intestine tissue (b) Intestine tissue fused by Ring electrode with the RF power of 120 W, welding time of 8 s, and compression force of 20 N. (c) Intestine tissue fused by the novel electrode with the RF power of 120 W, welding time of 8 s and compression force of 20 N.

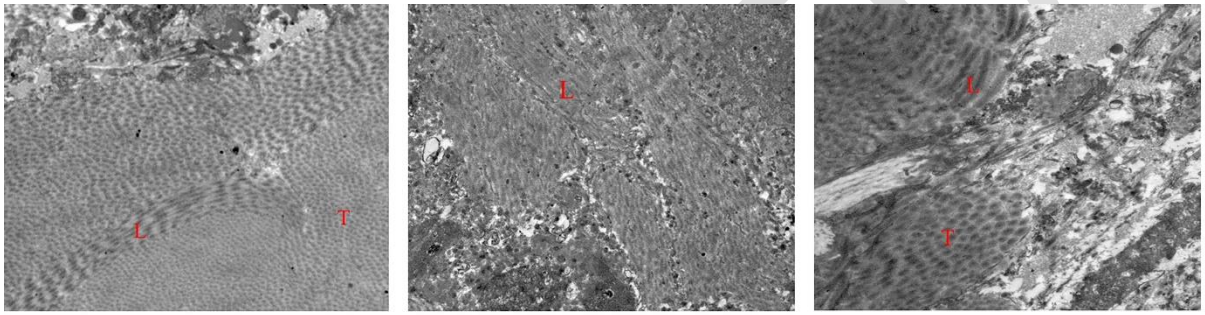

Figure.11 Transmission electron microscope image of fused intestinal tissue (a) Normal intestine tissue (b) Intestine tissue fused by Ring electrode with the RF power of 120 W, welding time of 8 s, and compression force of 20 N. (c) Intestine tissue fused by the novel electrode with the RF power of 120 W, welding time of 8 s and compression force of 20 N. T, transverse collagen fibrils; L, longitudinal collagen fibrils

4. Discussion

Based on the novel biodegradable electrode, we executed ex-vivo experiments of intestinal tissue fusion to authenticate the feasibility and effectiveness of the device, and the results showed that under the weld conditions of RF energy output power of 120 W, welding durations of 8 s and applied compression force of 20 N, the highest biomechanical strength could be obtained with the anastomotic tensile force of 11.8±2.01 N, the burst pressure of 89.6±6.79 mmHg, which is higher than traditional Ring electrode group with the anastomotic tensile force of 9.7±1.47 N, the burst pressure of 84.0±5.99 mmHg. Although the biomechanical strength of the anastomotic area welded by the two electrodes was not significantly different (p=0.076>0.05 for tensile force, p=0.251>0.05 for burst pressure) under the optimal weld combinations (Table2, group 1), the hollow structure of the novel electrode reduced section of

the middle fusion area by nearly 40% compared to Ring electrode (figure 7(a)).

Under the compression force of 20 N, the maximum deformation and maximum Von Mises stress of the novel electrode are 0.11 mm and 154.75 MPa, respectively. The maximum strain of the novel electrode is about 1.5%. The yield strength and elongation of the degradable magnesium alloy material used for the novel electrode are 320~380 MPa and 8%~18%, respectively indicating that the mechanical strength of the novel electrode is acceptable [2].

To better assess the performance of the proposed novel electrode, the tensile force of normal intestinal tissue was acquired by a universal testing machine with the approximate maximum force of 23 N. It was worth noting that the tensile force of the normal intestinal tissue is less than 20 N as it began to rupture. The biomechanical strength of the fused intestinal tissue greater than one-third that of normal intestinal tissue is considered safe, i.e. the tensile force of the fused intestinal tissue needs to be at least greater than 6 N [20], [31]. Due to the limitation of the range of the burst pressure measuring device used in this paper, the burst pressure of normal intestinal tissue is not obtained through experiments, but acquired through literature, and the minimum burst pressure of the fused intestinal tissue needs to be approximately greater than 30 mmHg [20], [31]. The fused intestinal tissue welded by our proposed novel electrode meets the requirements.

The temperature distribution and tissue thermal damage were investigated by finite element analysis under the weld conditions of RF energy output power of 120 W, welding durations of 8 s and applied compression force of 20 N, which leads to the highest biomechanical strength of the anastomotic area. The error between the temperature of the thermocouple probe in the welding experiments and the temperature of the domain point probe in the finite element analysis is lower than 8%, which indicates that the established finite element model is reliable. And the area of intestinal tissue with temperature above 60 °C during the fusion process is defined as an effective welding area for intestinal anastomosis.

The thermal conductivity of intestinal tissue would change when compression pressure was loaded, leading to a higher temperature at the junction between the compressed area and the uncompressed area of the intestinal tissue, which could explain the phenomenon that the junction between the compressed area and the uncompressed area tend to rupture in the welding experiments. As there is no uniform standard for evaluating tissue thermal injury in experiments, for the infrared thermal imaging monitoring results, the area with temperature higher than 60 °C is considered to suffer from thermal tissue damage [11], [27]. Thus the thermal damage range is obtained in experiments. Although the evaluation methods of tissue thermal damage in experiments and simulations are different, they all come to the same conclusion, that is, the

novel electrode can significantly reduce tissue thermal damage compared to the Ring electrode.

Compared to normal intestinal tissue which shows clear layered structure of serosa, muscle layer, sub-mucosa, and mucosa respectively, and presents regular arrangement of collagen fibers in the transverse and longitudinal directions, the anastomosis area is more tightly connected with collagenic crosslink, which demonstrates that satisfactory fusion was achieved. In future work, animal experiments will be carried out to further verify the performance of the novel electrode.

5. Conclusions

In this paper, we developed a novel electrode to assess its ability in RF-induced intestinal anastomosis using ex-vivo experiments and the finite element method. Compared to our previously proposed electrode, higher biomechanical strength of the fusion area is obtained with the tensile force of 11.8±2.01 N and burst pressure of 89.6±6.79 mmHg respectively, as well as less tissue thermal damage for the novel electrode group. Besides, the two layers of tightly connected intestinal tissue with collagenic crosslink for the fusion area could be observed by histopathological examination and transmission electron microscopy. Our study shows that the proposed novel electrode could achieve balance between anastomotic strength and tissue thermal damage for radiofrequency-induced intestinal anastomosis.

References

[1] DIENER M.K., SEILER C.M., ROSSION I., KLEEFF J., GLANEMANN M., BUTTURINI G., TOMAZIC A., BRUNS C.J., BUSCH O.R., FARKAS S., *Efficacy of stapler versus hand-sewn closure after distal pancreatectomy (dispact): A randomised, controlled multicentre trial*, The. Lancet., 2011, 377, 1514-1522.

[2] DING W., *Opportunities and challenges for the biodegradable magnesium alloys as next-generation biomaterials*, Regen. Biomater., 2016, 3, 79-86.

[3] DODDE R.E., BULL J.L., SHIH A.J., *Bioimpedance of soft tissue under compression and applications to electrosurgery*, Physiol. Meas., 2012, 33(6), DOI: 10.1088/0967-

3334/33/6/1095.

[4] DODDE R.E., MILLER S.F., GEIGER J.D., SHIH A.J., *Thermal-electric finite element analysis and experimental validation of bipolar electrosurgical cautery*, J. Manuf. Sci. E-T. Asme., 2008, 130(2), DOI: 10.1115/1.2902858.

[5] ELZAYAT S., ELSHERIF H., AOUF M., *Trans-oral endoscopic assisted radio-frequency for adenoid ablation; a randomized prospective comparative clinical study*, Auris. Nasus. Larynx., 2021, 48, 710-717.

[6] FERRERO S., STABILINI C., BARRA F., CLARIZIA R., ROVIGLIONE G., CECCARONI M., *Bowel resection for intestinal endometriosis*, Best. Pract. Res. Cl. Ob., 2021, 71, 114-128.

[7] GONZÁLEZ-SUÁREZ A., TRUJILLO M., BURDÍO F., ANDALUZ A., BERJANO E., *Could the heat sink effect of blood flow inside large vessels protect the vessel wall from thermal damage during RF-assisted surgical resection?*, Med. Phys., 2014, 41(8), DOI: 10.1118/1.4890103.

[8] GUO L., YU L., ZHAO Q., GONG X., XIE H., YUAN G., LI B., WAN X., *Biodegradable jdbm coating stent has potential to be used in the treatment of benign biliary strictures*, Biomed. Mater., 2021, 16(2), DOI: 10.1088/1748-605X/abda88.

[9] HOERMANN H., SCHLEBUSCH H., *Reversible and irreversible denaturation of collagen fibers,* Biochemistry., 1971, 10, 932-937.

[10] HOLMER C., WINTER H., KRÖGER M., NAGEL A., JAENICKE A., LAUSTER R., KRAFT M., BUHR H.J., RITZ J.P., *Bipolar radiofrequency-induced thermofusion of intestinal anastomoses-feasibility of a new anastomosis technique in porcine and rat colon*, Langenbecks. Arch. Surg., 2011, 396, 529-533.

[11] HU Z., ZONG N., SONG C., ZHOU Y., TU L., MAO L., *Intestinal tissue fusion based on radiofrequency energy*, J. Med. Biomech., 2021, 36, 790-796 (in Chinese).

[12] KRAMER E.A., RENTSCHLER M.E., *Energy-based tissue fusion for sutureless closure: applications, mechanisms, and potential for functional recovery*, Annu. Rev. Biomed. Eng., 2018, 20, 1-20.

[13] MAHAPATRO A., MATOSNEGRON T.D., GOMES A.S., *Nanostructured self assembled monolayers on magnesium for improved biological performance*, Mater. Technol., 2016, 31, 818-827.

[14] MAO L., ZHU H., CHEN L., ZHOU H., YUAN G., SONG C., *Enhancement of corrosion resistance and biocompatibility of Mg-Nd-Zn-Zr alloy achieved with phosphate coating for vascular stent application*, J. Mater. Res. Technol., 2020, 9, 6409-6419.

[15] PAN H., PAN F., WANG X., PENG J., GOU J., SHE J., TANG A., *Correlation on the electrical and thermal conductivity for binary Mg-Al and Mg-Zn alloys*, Int. J. Thermophys., 2013, 34, 1336-1346.

[16] PAWLIKOWSKI M., NIERODA A., *Comparative analyses of blood flow through mechanical trileaflet and bileaflet aortic valves*, Acta. Bioeng. Biomech., 2022, 24, 141-152.

[17] PEARCH J.A., *Comparative analysis of mathematical models of cell death and thermal damage processes*, Int. J. Hyperthermia., 2013, 29, 262-280.

[18] PENNES H.H., *Analysis of tissue and arterial blood temperatures in the resting human forearm*, J. Appl. Physiol., 1948, 1, 93-122.

[19] SMULDERS J.F., DEHINGH I., STAVAST J., JACKIMOWICZ J., *Exploring new technologies to facilitate laparoscopic surgery: creating intestinal anastomoses without sutures or staples, using a radio-frequency-energy-driven bipolar fusion device*, Surg. Endosc., 2007, 21, 2105-2109.

[20] SODERGREN M., CLARK J., BEARDSLEY J., BRYANT T., HORTOB K., DARZI A., TEARE J., *A novel flexible endoluminal stapling device for use in NOTES colotomy closure: a feasibility study using an ex vivo porcine model*, Surg. Endosc., 2011, 25, 3266-3272.

[21] SUNG H., FERLAY J., SIEGEL R.L., LAVERSANNE M., SOERJOMATARAM I., JEMAL A., BRAY F., *Global cancer statistics 2020: Globocan estimates of incidence and mortality worldwide for 36 cancers in 185 countries*, CA-Cancer. J. Clin., 2021, 71, 209-249.

[22] TRUJILLO M., BERJANO E., *Review of the mathematical functions used to model the temperature dependence of electrical and thermal conductivities of biological tissue in radiofrequency ablation*, Int. J. Hyperthermia., 2013, 29, 590-597.

[23] TU L., ZHOU Y., SONG C., LI Y., CHEN L., XUE Y., *Preliminary study of a control algorithm for radiofrequency-induced intestinal tissue fusion*, Int. J. Hyperthermia., 2019, 36, 1296-1305.

[24] TU L., ZHOU Y., WANG P., WANG H., MAO L., HOU J., LIU Z., SONG C., *Minimizing thermal damage using self-cooling jaws for radiofrequency intestinal tissue fusion*, Minim. Invasiv. Ther., 2023, 32, 33-41.

[25] WANG Q., YUAN H., GUO M., MENG L., LONG Z., LONG Y., YANG H., *Three-dimensional finite element analysis of a novel interzygapophyseal fusion device for lower cervical spine*, Acta. Bioeng. Biomech., 2022, 24, 187-193.

[26] WANG Z., ZHU S., WANG L., CHANG L., WANG J., LI J., GUAN S., *Preparing a novel magnesium-doped hyaluronan/polyethyleneimine nanoparticle to improve endothelial functionalisation*, Iet. Nanobiotechnol., 2020, 14, 142-147.

[27] YAN S., WU X., WANG W., *Theoretical and experimental analysis of amplitude control ablation and bipolar ablation in creating linear lesion and discrete lesions for treating atrial fibrillation*, Int. J. Hyperther., 2017, 33, 608-616.

[28] ZANG L., ZHOU Y., KANG J., SONG C., *Effect of the combination of different electrode spacings and power on bipolar radiofrequency fat dissolution: a computational and experimental study*, Lasers. Surg. Med., 2020, 52, 1020-1031.

[29] ZHANG C., LIU H., TAN R., LI H., *Interaction model between capsule robot and intestine based on nonlinear viscoelasticity*, P. I. Mech. Eng. H., 2014, 228, 287-296.

[30] ZHAO L., SONG C., WANG Z., ZHOU Y., LI X., ZHU W., CUSCHIERI A., *Novel concave–convex electrode for colonic anastomoses by radiofrequency thermo-fusion*, Surg. Endosc., 2015, 29, 1809-1816.

[31] ZHOU H., HAN S., CHEN J., HUANG D., PENG L., NING J., LI Z., *A feasibility study of closing the small bowel with high-frequency welding device*, J. Biomedical. Eng., 2014, 31, 1332-1335 (in Chinese).

Figure captions

Figure.1 Mechanical structure and working flow chart of the novel electrode
(a) Mechanical structure of traditional Ring electrode (b) Mechanical structure of novel electrode (c) Working flow chart of the novel electrode.

Figure.2 Schematic diagram of force loading method.

Figure.3 Geometry of the finite element model for temperature distribution and tissue thermal damage. (a) The overall chart of the finite element model. (b) The fusion model of the traditional Ring electrode. (c) The fusion model of the novel electrode.

Figure.4 Intestinal tissue fusion platform.

Figure.5 Strength test of anastomotic area (a) Schematic diagram of burst pressure test (b) Tensile force test of the fused intestinal tissue (c) Tensile force test of normal intestinal tissue.

Figure.6 Finite element analysis results of the novel electrode after loading pressure (a) Deformation contour of the novel electrode (b) Von Mises stress contour of the novel electrode.

Figure.7 Prototype of the novel electrode and biomechanical strength of intestinal tissue (a) Prototype of the Ring electrode (up), prototype of the novel electrode (down) (b) Mechanical strength test results of the anastomotic area (c) Tensile force test result of normal intestinal tissue. (d) Top view of intestinal tissue deformation in the anastomosis area for the novel electrode fusion model. (e) The sectional view of intestinal tissue deformation in the anastomosis area for the novel electrode fusion model.

Figure.8 Temperature distribution contours of intestinal tissue fused under the condition of compression force of 20 N, RF energy of 120 W, and welding duration of 8 s. (a) Temperature distribution contours of intestinal tissue fused by Ring electrode (b) Temperature distribution contours of intestinal tissue fused by the novel electrode (c) The curve of the temperature of the domain point probe in finite element model and thermocouple probe in the experiment, respectively. C, intestinal tissue under compression by the two electrodes; U, uncompressed intestinal tissue.

Figure.9 Tissue thermal damage under the condition of compression force of 20 N, RF energy of 120 W, and welding duration of 8 s. (a) Tissue thermal damage distribution contours of intestinal tissue fused by Ring electrode (b) Tissue thermal damage distribution contours of intestinal tissue fused by the novel electrode (c) Percentage of necrotic tissue. C, intestinal tissue under compression by the two electrodes; U, uncompressed intestinal tissue.

Figure.10 Histopathological examination of anastomosis area. (a) Normal intestine tissue (b) Intestine tissue fused by Ring electrode with the RF power of 120 W, welding time of 8 s, and compression force of 20 N. (c) Intestine tissue fused by the novel electrode with the RF power of 120 W, welding time of 8 s and compression force of 20 N.

Figure.11 Transmission electron microscope image of fused intestinal tissue (a) Normal intestine tissue (b) Intestine tissue fused by Ring electrode with the RF power of 120 W, welding time of 8 s, and compression force of 20 N. (c) Intestine tissue fused by the novel electrode with the RF power of 120 W, welding time of 8 s and compression force of 20 N. **T**, transverse collagen fibrils; **L**, longitudinal collagen fibrils.